ACS Energy LETTERS

http://pubs.acs.org/journal/aelccp

Ultrafast Sintering of Solid-State Electrolytes with Volatile Fillers

Min Hong,‖ Qi Dong,‖ Hua Xie,‖ Bryson Callie Clifford, Ji Qian, Xizheng Wang, Jian Luo, and Liangbing Hu*

Cite This: *ACS Energy Lett.* 2021, 6, 3753–3760

Read Online

ACCESS | Metrics & More | Article Recommendations | Supporting Information

ABSTRACT: **Enhancing the performance of ceramic solid-state electrolytes (SSEs) often relies on incorporating effective fillers. However, the choice of fillers is often limited to only a few highly stable ones, as the long-term sintering by conventional methods often leads to severe loss of volatile components. Herein, we develop an ultrafast sintering method for SSEs with volatile fillers toward a dense and high-performance membrane. Using Ta-doped $Li_7La_3Zr_2O_{12}$ (LLZTO) as a model system, we sinter a Li_3N/LLZTO composite SSE, which shows a higher relative density, a higher ionic conductivity, and a reduced electronic conductivity compared to the pristine LLZTO. In contrast, no Li_3N can be observed in the membrane sintered by a conventional furnace due to its high volatility. This study opens up a new route for the rational selection of fillers in a much broader space toward synthesizing high-quality and high-performance ceramic SSEs.**

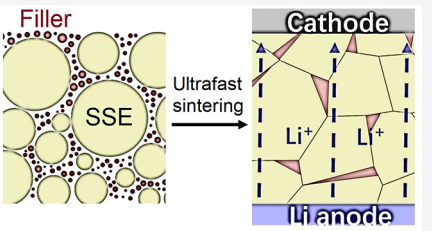

It has become more and more difficult for conventional Li-ion battery technologies based on a liquid or gel electrolyte to meet the ever-increasing societal demand.[1,2] Solid-state electrolytes (SSEs) made by ion-conducting ceramics hold great promise for the next-generation Li battery technologies with better safety and higher energy density.[3−5] A range of ceramic SSEs, such as perovskite-type $Li_{3x}La_{2/3-x}TiO_3$, NASICON-type $Li_{1.3}Al_{0.3}Ti_{1.7}(PO_4)_3$, and $Li_{1+x}Al_xGe_{2-x}(PO_4)_3$, and garnet-type $Li_7La_3Zr_2O_{12}$ (LLZO) and its derivatives have been studied owing to their appealing ionic conductivity (up to 10^{-3} S cm^{-1}), wide electrochemical window (up to 6 V), good chemical stability against Li metal, and excellent mechanical properties (up to 20 GPa).[6−10] However, their application in all-solid-state batteries has been hindered by the presence of voids, gaps, and pinholes upon sintering, as these defects are vulnerable spots for the penetration of Li dendrites, leading to thermal runaway, fire, and even explosion.[11−13] This problem is particularly acute when operating cells at medium to high current densities and long durations, making the ceramic SSEs incapable of realizing their high promise.[14,15] Among intensive efforts to address such an issue, sintering SSEs with inorganic fillers and sintering aids such as Al_2O_3, SiO_2, MgO, CaO, BaO, LiF, LiCl, Li_3BO_3, Li_3PO_4, and BN has proven a viable solution to increase density and block the dendrite penetration.[16−23] However, many promising fillers and sintering aids were previously excluded due to their susceptibility of decomposition and sublimation during the prolonged heating of conventional sintering methods.[24−26]

Herein, we report an ultrafast liquid-phase sintering method with highly volatile sintering aids (also as fillers) that are unattainable by conventional methods. Our approach uses Joule heating of carbon materials to reduce the heating time from hours to seconds with fast temperature ramping and cooling (10^3∼10^4 K/s), which enables sintering a mixture of SSE and filler with minimal volatilization of materials. Our sintering technique is superior compared to the conventional sintering method in terms of achieving better density, lower electrical conductivity, and higher ionic conductivity. Notably, the total sintering process can be completed within tens of seconds, comparable to the ultrafast sintering methods such as spark plasma sintering and flash sintering. To demonstrate the utility of our method, we selected Li_3N as the sintering aid to be incorporated in a Ta-doped $Li_7La_3Zr_2O_{12}$ (LLZTO) SSE. Li_3N is a good sintering aid as well as a desired filler candidate for composite SSEs due to its good ionic conductivity (>10^{-4} S cm^{-1}) and low electrical conductivity (<10^{-12} S cm^{-1}), yet its application was previously hindered due to its high volatility.[27−29] Compared to the conventional approaches that cannot incorporate Li_3N without severe losses, we used our ultrafast liquid-phase sintering method and achieved a highly dense Li_3N/LLZTO membrane at ∼1600 K in only 20

Received: July 25, 2021
Accepted: September 17, 2021
Published: September 30, 2021

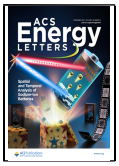

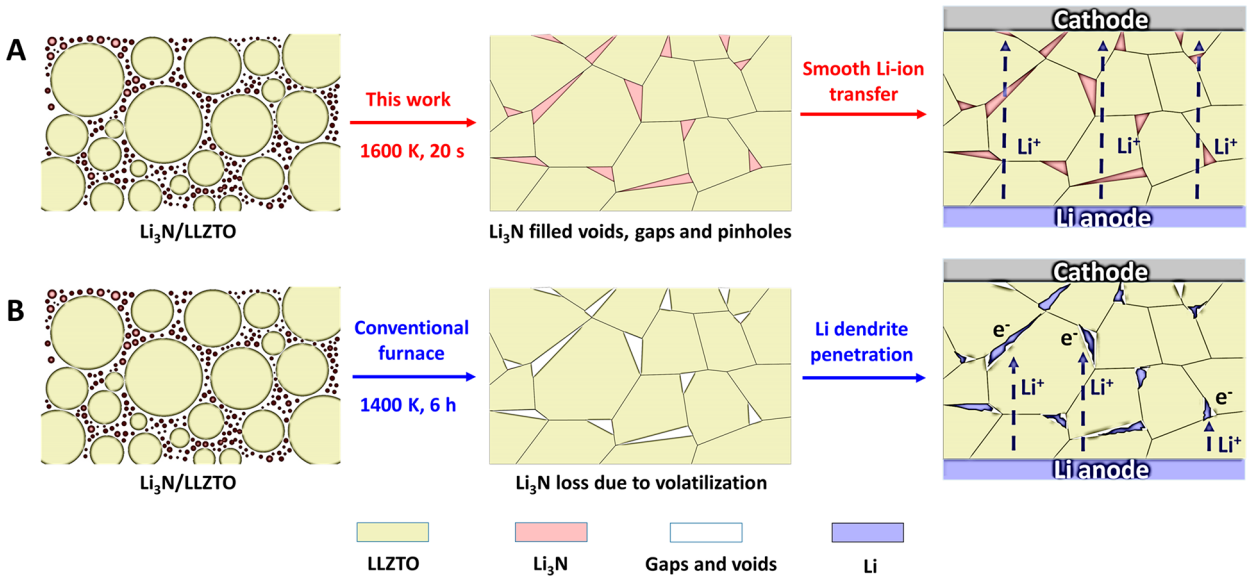

Figure 1. Schematic comparison between our ultrafast sintering method and conventional furnace sintering for the synthesis of composite SSEs. (A) Our ultrafast sintering occurs at a high temperature of 1600 K for only 20 s, limiting the loss of volatile fillers and sintering aids toward a dense microstructure. The yellow color refers to the SSEs, and the pink color between grains refers to the fillers. After sintering, the fillers fill the voids and gaps as well as coat the grains to improve the Li-ion diffusion. (B) In comparison, conventional furnace sintering causes a heavy loss of volatile substances where large gaps, voids, and pinholes are often created, which is represented by the white color between the grains after sintering. Li ions combine with electrons more easily in the gaps, voids, and pinholes, which eventually causes cell failure.

s. With this method, we avoided the volatilization of Li_3N (remained as a liquid phase at ~1600 K), which was found to fill the voids and pinholes as well as to wet the grains toward a dense microstructure. In comparison, no Li_3N was observed in the membrane sintered by using a conventional furnace. Owing to the successful incorporation of Li_3N, the composite SSE membrane showed a high relative density of 95%, ionic conductivity of 1.09×10^{-3} S cm^{-1}, and a low electronic conductivity of 2×10^{-9} S cm^{-1}, all superior compared to the LLZTO membrane. In addition, a reduced areal specific resistance (ASR) of 35 Ω·cm^2 and an improved critical current density (CCD) of 2.3 mA cm^{-2} were measured, also better than the LLZTO membrane. The Li|Li_3N/LLZTO|Li cell can be cycled for 500 h with a low overpotential of 8 mV at a current density of 0.2 mA cm^{-2} and for 160 h at a current density of 0.5 mA cm^{-2}, both much longer than the Li|LLZTO|Li cell. This study enables the rational selection of fillers and sintering aids in a much broader space for microstructure optimization of ceramic SSEs.

The core concept of our work is highlighted in Figure 1, which compares our ultrafast sintering with the conventional furnace sintering using a composite SSE with LLZTO and Li_3N as an example. Our ultrafast sintering process occurs at a relatively high temperature of 1600 K for only 20 s to create a dense microstructure, where the gaps, voids, and pinholes between the grains that lack a neck connection can be filled with Li_3N. The high temperature used in our approach could render an accelerated sintering rate with surface energy being the main driving force, where LLZTO particles formed "neck bonding" and then densified by removing the voids.[8,30] Importantly, the liquid phase of Li_3N during high-temperature sintering can help rearrange particles via capillary pressure, thereby reducing porosity.[31−33] Compared to previous furnace-based sintering approaches, this process is benign for most fillers and sintering aids including the highly volatile ones, which can readily be decomposed and evaporated unless using a short heating time.[26] The successful incorporation of Li_3N can help heal the defects and fill the voids, gaps, and pinholes as well as wrap the grains, together increasing the relative density and suppressing Li dendrite penetration (Figure 1A). In contrast, using a conventional furnace to sinter SSEs usually takes several hours due to the limited temperature as well as the slow ramping and cooling rates. The long sintering duration limits the choices of fillers and sintering aids to only the highly stable ones, prohibiting the rational selection of desirable candidates in a broader space. When sintering SSE powders with volatile substances using a conventional furnace, large gaps, voids, and pinholes can easily form due to the severe evaporation and decomposition of fillers and sintering aids such as Li_3N (Figure 1B). These gaps, voids, and pinholes are vulnerable spots for Li dendrite penetration.

In this work, we selected the LLZTO as a model SSE material due to its high conductivity, wide electrochemical window, and good processability. The highly Li^+-conductive but also highly volatile Li_3N was chosen as the filler to be incorporated in the composite SSE using our method.[33] Li_3N has shown excellent performance when serving as a solid electrolyte interface (SEI) component or an artificial SEI layer.[34] However, Li_3N can be easily decomposed and evaporated during long-term sintering, for which it has never been used as a filler or sintering aid in SSEs. In a typical process, a mixture of LLZTO and Li_3N powders was milled together thoroughly in a controlled weight ratio (1 wt %), which was then uniaxially pressed into green pellets. The pellets were sandwiched between two pieces of Joule-heated carbon felt, sintered using the aforementioned condition, and characterized by microscopic tools.[30] The scanning electron microscope (SEM) image of the fractured Li_3N/LLZTO SSE membrane shows a highly uniform and dense microstructure throughout the whole cross section (Figure 2A). After

https://doi.org/10.1021/acsenergylett.1c01554
ACS Energy Lett. 2021, 6, 3753−3760

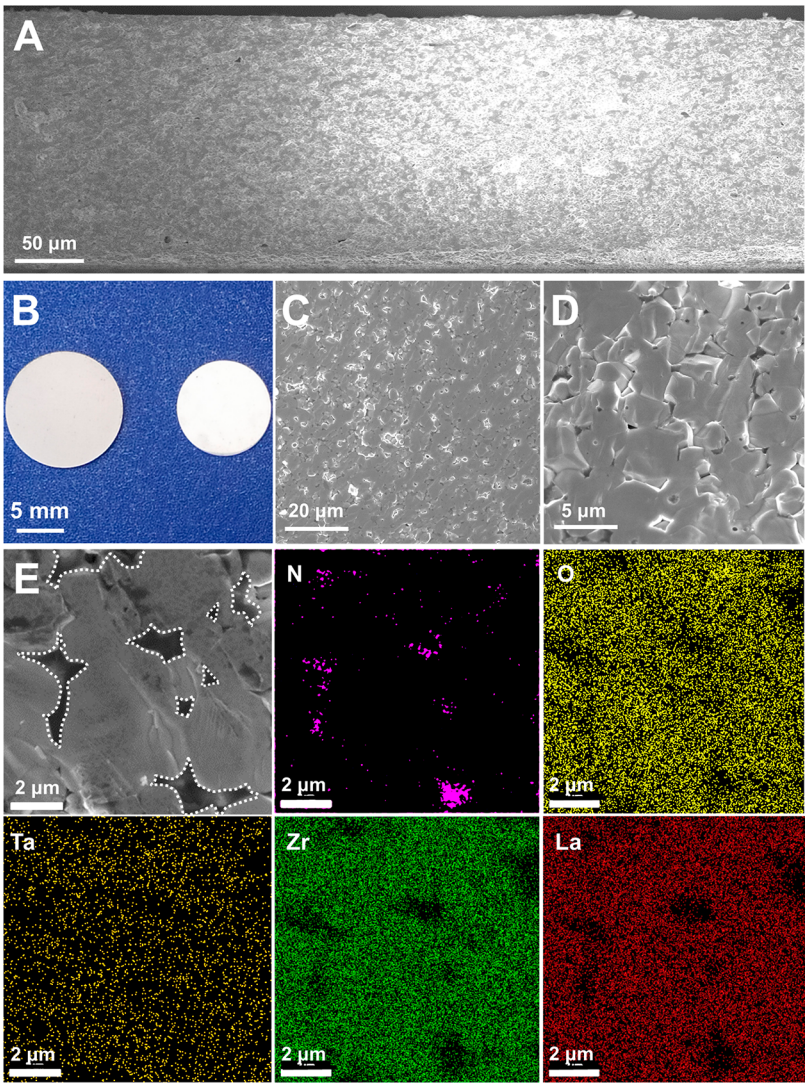

Figure 2. Microscopic characterization of the fractured surface of the Li_3N/LLZTO SSE membrane prepared by our ultrafast sintering method. (A) SEM image (secondary electron) of the fractured Li_3N/LLZTO SSE membrane. (B) Digital image of the Li_3N/LLZTO SSE membrane before (left) and after (right) the rapid sintering process. (C,D) SEM images of the fractured Li_3N/LLZTO SSE membrane at higher magnifications. (E) Elemental mapping of the fractured Li_3N/LLZTO SSE membrane.

sintering, the membrane shrank by 19.8 and 22.5% along the axial and radial directions, respectively, leading to a relative density of 95%, which is slightly higher than the pure LLZTO membrane sintered under the same condition (93%) (Figure 2B). The membrane remained flat and smooth without any observable deformation owing to the controlled grain growth. A dense microstructure can also be observed in the magnified views under SEM, where most grains formed neck bonding with only a few void- and pinhole-like spots (Figure 2C,D). Such a morphology is typical for garnet-based SSEs in the literature reports.

To better locate the Li_3N filler, we used energy-dispersive spectroscopy (EDS) to map the elemental distribution of N, O, Ta, Zr, and La on a selected spot of the fractured Li_3N/LLZTO SSE membrane (Figure 2E). Interestingly, the N elemental map shows that the Li_3N filler was primarily distributed in the voids, gaps, and pinholes. In addition, while the O elemental map overlaps with those of Ta, Zr, and La, which belong to the LLZTO component, they do not overlap with but compensate the N elemental map, indicating little cross-diffusion. The SEM image of the Li_3N/LLZTO SSE membrane surface demonstrates that the liquid-phase Li_3N conformally wets the grains of the LLZTO during sintering (Figure S1). The elemental maps of O, Ta, Zr, and La also overlap with each other and so does the elemental map of N, as the signal intensity generally follows the height profile of the sample, especially on an unpolished nonflat surface. These mapping results indicate that the Li_3N filler was distributed among the voids, gaps, and pinholes as well as coated the surface of the LLZTO grains.

The incorporation of the highly volatile Li_3N filler is unattainable by conventional furnace sintering. As a control experiment, we sintered the pellet made by an identical process using a furnace at 1150 °C for 6 h. While the microstructure is comparably dense (~93% relative density), the elemental mapping results showed almost no N signal (Figure S2), indicating severe loss of Li_3N during the long-term sintering. As another control experiment, we sintered pellets containing different loadings of the Li_3N filler ranging from 2−5 wt %. SEM images of fractured Li_3N/LLZTO SSE membranes show an increase of thickness of grain boundaries and eventually a porous microstructure likely due to the loss of an excess

https://doi.org/10.1021/acsenergylett.1c01554
ACS Energy Lett. 2021, 6, 3753−3760

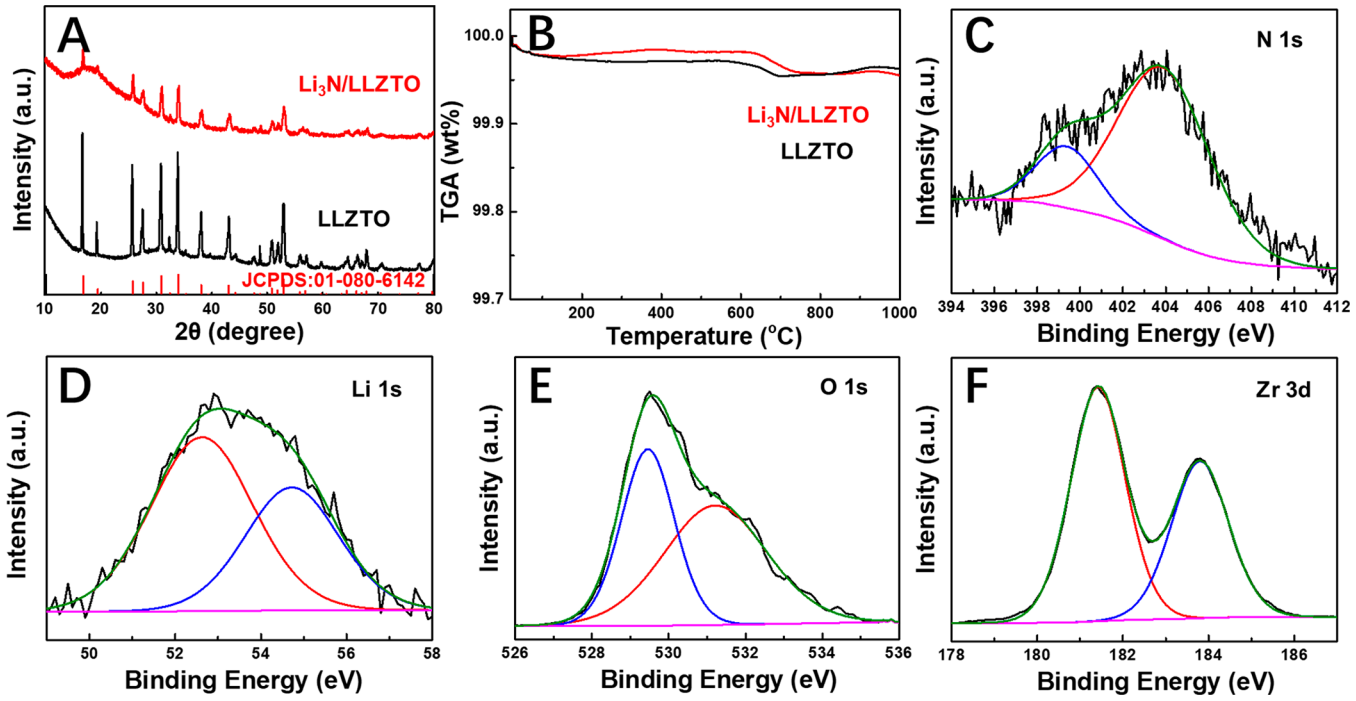

Figure 3. Characterization of the SSE membranes synthesized by our ultrafast sintering method. (A) XRD analysis of the LLZTO SSE membranes with and without Li_3N, in comparison with the standard diffraction pattern of $Li_{6.5}La_3Zr_{1.45}Ta_{0.55}O_{12}$ (JCPDS: 01−080−6142). The XRD pattern is plotted in a logarithmic scale. (B) TGA curves of the LLZTO SSE membranes with and without Li_3N. XPS spectra of (C) N 1s, (D) Li 1s, (E) O 1s, and (F) Zr 3d for the Li_3N/LLZTO composite SSE membrane.

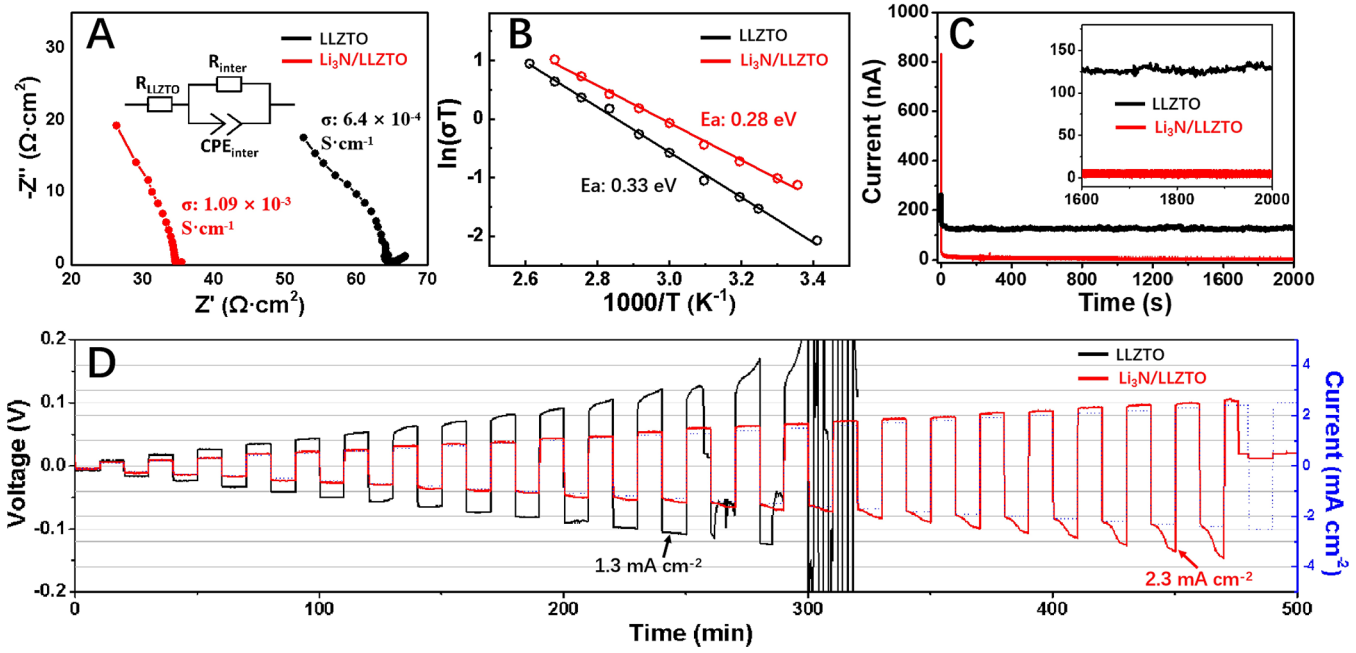

Figure 4. Electrochemical performance of symmetric cells made by Li_3N/LLZTO and LLZTO SSE membranes. (A) Ionic conductivities of Li_3N/LLZTO and LLZTO by EIS measurement. (B) Activation energies of Li_3N/LLZTO and LLZTO. (C) Electronic conductivities of Li_3N/LLZTO and LLZTO. (D) Critical current density (CCD) test for the symmetric cells made by Li_3N/LLZTO and LLZTO SSE membranes.

amount of Li_3N (Figure S3). Although the segregated LLZTO grains even by 2 wt % Li_3N filler may not be favorable for battery applications, this experiment helped us explore the loading threshold (~5 wt %) of the Li_3N filler to maintain a dense microstructure with our ultrafast sintering method.

We further characterize the physiochemical properties of the LLZTO SSE membranes synthesized by our ultrafast sintering method. X-ray diffraction (XRD) was carried out for the LLZTO with and without the Li_3N filler. Both of their XRD patterns agree with the desired cubic phase of LLZTO (JCPDS: 01−080−6142), suggesting successful synthesis from

https://doi.org/10.1021/acsenergylett.1c01554
ACS Energy Lett. 2021, 6, 3753−3760

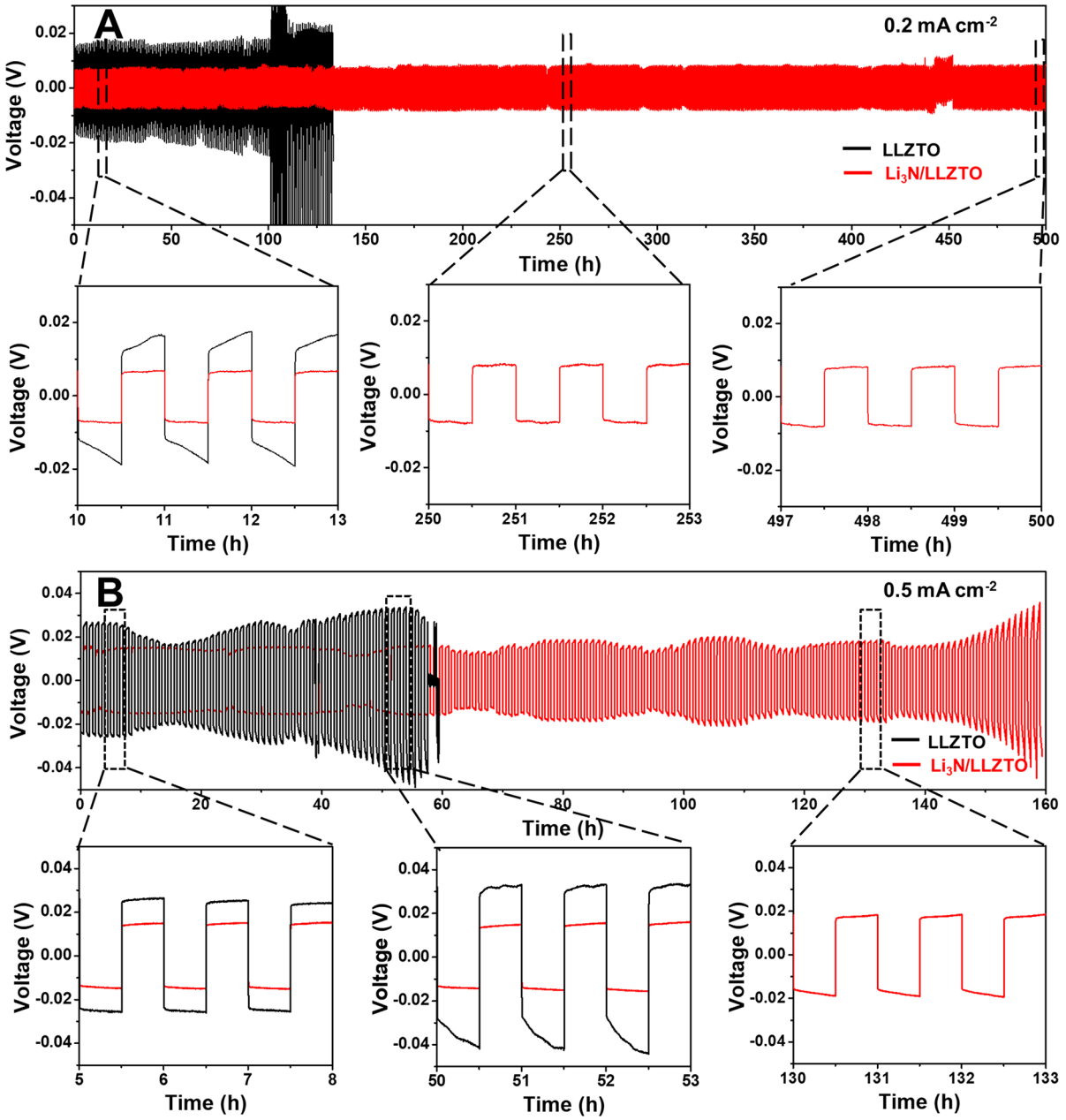

Figure 5. Galvanostatic cycling performance of symmetric cells made by Li_3N/LLZTO and LLZTO SSE membranes. (A) Galvanostatic cycling of the Li|LLZTO|Li and Li|Li_3N/LLZTO|Li cells at 0.2 mA cm^{-2}. (B) Galvanostatic cycling of the Li|LLZTO|Li and Li|Li_3N/LLZTO|Li cells at 0.5 mA cm^{-2}.

powders to a membrane (Figure 3A). Li_3N was not observed by XRD for the Li_3N/LLZTO composite SSE membrane, likely due to the low amount. The membranes made of LLZTO with and without the Li_3N filler synthesized by our ultrafast sintering method were also characterized by thermogravimetric analysis (TGA). Due to the dense microstructure where Li_3N is well trapped, no obvious difference can be observed by comparing the two membranes (Figure 3B). X-ray photoelectron spectroscopy (XPS) was next conducted for the Li_3N/LLZTO composite SSE membrane for various elements. The deconvoluted N 1s spectrum shows a major peak and a minor peak, which we attributed to the Li_3N filler and its potential interaction with the LLZTO matrix (Figure 3C). In addition, the inevitable air exposure during sample transfer for the XPS measurement likely causes sample contaminations that complicate the data analysis. Despite the artifacts, the broad peak centered at 403 eV is likely composed of N−H and N−O species, while the other small peak centered at 398.5 eV also originated from Li_3N fillers.[35,36] The deconvoluted Li 1s spectrum is consistent with the electronic states of Li in both LLZTO and Li_3N (Figure 3D).[37] The O 1s spectrum shows a minor peak with a binding energy at 529.2 eV associated with the structural oxygen and a major peak with a binding energy at 531.3 eV associated with the absorbed O_2 from the environment (Figure 3E).[38] Lastly, Zr 3d spectrum exhibits two deconvoluted peaks, which can be attributed to Zr^{4+} $3d_{3/2}$ at 183.8 eV and Zr^{4+} $3d_{5/2}$ at 181.4 eV, respectively (Figure 3F).[30]

As discussed above, the Li_3N fills the voids, gaps, and pinholes as well as coats the grains of LLZTO, thereby

https://doi.org/10.1021/acsenergylett.1c01554
ACS Energy Lett. 2021, 6, 3753−3760

potentially improving the electrochemical properties of the SSE membrane. We used a symmetric cell configuration to characterize the Li_3N/LLZTO composite membrane and the LLZTO membrane as a control. Electrochemical impedance spectroscopy (EIS) revealed a decrease of areal specific resistance (ASR) from 63 to 35 $\Omega \cdot cm^2$ and an increase of ionic conductivity from 6.4×10^{-4} to 1.09×10^{-3} S cm^{-1} at 298 K after the Li_3N filler was incorporated with LLZTO (Figure 4A). The activation energy (E_a) of Li^+ conduction for the Li_3N/LLZTO was then measured to be 0.28 eV from 298 to 373 K according to the Arrhenius law (i.e., $\sigma T \approx \exp(-E_a/KT)$), which is 0.05 eV lower than that of the pure LLZTO (Figure 4B). In addition to the ionic conductivity, another key factor for the overall performance of an SSE membrane is the electronic conductivity, which was found to have an impact on the Li dendritic growth and penetration.[39−41] Figure 4C shows the current−time profiles of the SSE membranes with and without the Li_3N filler, which were measured using the blocking electrode method under DC polarization at 1 V. The current first decreases and then plateaus as a result of electrical leak. The electronic conductivities were calculated to be 3.5×10^{-8} and 2×10^{-9} S cm^{-1} at 298 K for LLZTO and Li_3N/LLZTO respectively. The electronic conductivity decreased by over an order of magnitude after Li_3N filler was incorporated, which suppresses the dendrite penetration and benefits the cycling stability. We characterized the critical current density (CCD) using a rate increment of 0.1 mA cm^{-2} and a duration of 10 min (Figure 4D). The Li|Li_3N/LLZTO|Li symmetric cell shows a much more stable performance and smaller overpotential compared with the Li|LLZTO|Li symmetric cell. The CCD values are 1.3 and 2.3 mA cm^{-2} for the Li|LLZTO|Li and the Li|Li_3N/LLZTO|Li symmetric cells, respectively, indicating the critical role played by the Li_3N filler and the successful incorporation by our ultrafast sintering method.

We further test the Li|LLZTO|Li and Li|Li_3N/LLZTO|Li cells under galvanostatic conditions to compare their long-term cycling stability. Using a current density of 0.2 mA cm^{-2} with an areal capacity of 0.1 mAh cm^{-2}, the Li|Li_3N/LLZTO|Li cell demonstrated stable operation for 500 h (Figure 5A). The magnified views show small overpotentials of only ∼8 mV, indicating facile Li plating and stripping processes. In comparison, the Li|LLZTO|Li symmetric cell showed a gradually increased overpotential and eventually shorted after ∼100 h of cycling operation (Figure 5A). In Figure 5B, when testing with a larger current density of 0.5 mA cm^{-2} and an areal capacity of 0.25 mAh cm^{-2}, the Li|Li_3N/LLZTO|Li cell still outperformed the LLZTO membrane in terms of cycling stability and overpotential. In particular, despite the fluctuations in the voltage profile, the Li|Li_3N/LLZTO|Li demonstrated a stable cycling performance for up to 150 h, in comparison with the 55 h by the Li|LLZTO|Li cell. Our ultrafast sintering method effectively incorporated the highly volatile Li_3N filler in the composite SSE, which improves the relatively density, ionic conductivity, and electrical resistivity, thereby offering a better CCD and cycling performance.

In this work, we report the successful synthesis of a composite SSE with highly volatile fillers such as Li_3N, which is unattainable by conventional methods. This is achieved by using an ultrafast sintering process by Joule heating of carbon materials, thereby largely reducing the sintering time from hours to seconds owing to the fast temperature ramping and cooling rates (10^3∼10^4 K/s). Using a model system featuring the highly volatile Li_3N filler and the LLZTO as the SSE, we used the ultrafast sintering method to create a dense and high-quality Li_3N/LLZTO membrane at ∼1600 K in only 20 s. The Li_3N filler was found to fill the voids and pinholes as well as coat the LLZTO grains, which resulted in a high relative density of 95%, a high ionic conductivity of 1.09×10^{-3} S cm^{-1}, and a low electronic conductivity of 2×10^{-9} S cm^{-1}. With the successful incorporation of Li_3N, higher CCD value and better cycling stability were measured for the composite SSE membrane as compared with the pure LLZTO membrane. In particular, the Li|Li_3N/LLZTO|Li cell cycled for 500 and 160 h at 0.2 and 0.5 mA cm^{-2}, respectively, both outperforming the Li|LLZTO|Li cell. This work paves a new route toward the rational compositional and structural design of ceramic SSEs and beyond. We envision this method to be widely applicable to a range of composite systems where multiple components with largely different physiochemical properties can be integrated in a highly efficient fashion.

MATERIALS AND METHODS

Starting Materials. The $Li_{6.5}La_3Zr_{1.45}Ta_{0.55}O_{12}$ green powders were prepared according to work reported previously.[42] In short, a mixture of precursors including LiOH·H_2O (99.9%, Sigma-Aldrich), La_2O_3 (≥99.9%, Sigma-Aldrich), ZrO_2 (99.9%, Sigma-Aldrich), and Ta_2O_5 (99.9%, Sigma-Aldrich) was mechanically ball-milled in isopropyl alcohol (IPA) overnight. Additional, 10 wt % excess of LiOH·H_2O was added to compensate the lithium evaporation during the last step of sintering. And 0.3 wt % of Al_2O_3 nanopowder was added to act as a sintering aid of the pellet. After milling, the precursor powders were calcined at 1193 K for 12 h in a muffle furnace with a ramping rate of 5 °C min^{-1}. The obtained calcined powders were ball-milled again and then mixed with Li_3N (99.9%, Sigma-Aldrich) by milling with different weight percentages. After fully milling, the composite powders were pressed using the stainless steel die into green pellets with a diameter of 10 mm and thickness of about 550 μm.

Ultrafast Sintering. The experimental setup was demonstrated in our previous work.[30] In a typical process, two pieces of carbon felt (Fuel Cell Earth, 8 × 1.5 cm) were fixed on the graphite holder. The high-temperature sintering process was implemented with an energy input from the DC power supply (StarPower, 0−100 V, 0−50 A) through the graphite holder to the carbon felt heating element. The carbon felt as the Joule heating element could be ramped to a high temperature in seconds by controlling the DC power supply. During the sintering process, the pressed LLZTO and Li_3N composite green pellets were placed on the heater; then, we ramped the temperature and kept it until the green pellets became dense. The preparation process of the composite pellets and subsequent sintering were conducted in an argon-filled glovebox. The sintered membranes cooled to room temperature within ∼3 s. The sintering process was recorded with the assistance of a digital camera (Canon 60D, 30 frames s^{-1}). A visible−near-infrared spectrometer (USB2000+, Ocean Optics) was adopted to collect the light emission of the heater, and then, its temperature was calculated as reported previously.[43]

Materials Characterization. The surface and fractured morphologies and elemental distribution of the sintered Li_3N/LLZTO composite electrolyte were observed using a Tescan GAIA SEM coupled with an energy-dispersive X-ray spectroscopy (EDS) detector at 10 kV. XRD data was collected by using a D8 Bruker Advanced XRD system with a Cu Kα

https://doi.org/10.1021/acsenergylett.1c01554
ACS Energy Lett. 2021, 6, 3753−3760

radiation source operated at 40 kV and 40 mA. XPS was performed on a Thermo ESCALAB 250. Thermogravimetric analysis (TGA) was performed on a Discovery SDT 650 thermal analyzer by TA Instruments.

Electrochemical Measurements. To test the electrochemical performance of the fabricated Li_3N/LLZTO composite electrolyte, a Li|Li_3N/LLZTO|Li symmetric cell was assembled by coating Li metal on both sides of the composite electrolyte.[30] EIS was measured at a frequency range from 100 mHz to 1 MHz with an amplitude of 10 mV. The Li^+ conductivity of the composite electrolyte was calculated according to the equation $\sigma = D/(A \times R)$, where D, A, and R refer to the thickness, area, and resistance of the electrolyte, respectively. Galvanostatic charging/discharging of the Li|Li_3N/LLZTO|Li symmetric cell was performed at different current densities with a step size of 30 min. The DC polarization was performed on a blocking electrode under a constant voltage of 1 V. Silver paste was coated on both sides of the composite electrolyte, and the Ag/electrolyte membrane/Ag was preheated at 200 °C for 30 min before the DC polarization test. All these electrochemical measurements were performed in an argon-filled glovebox using a BioLogic VMP3 potentiostat at room temperature.

■ ASSOCIATED CONTENT

Supporting Information

The Supporting Information is available free of charge at https://pubs.acs.org/doi/10.1021/acsenergylett.1c01554.

Additional characterizations of the Li_3N/LLZTO SSE membranes (PDF)

■ AUTHOR INFORMATION

Corresponding Author

Liangbing Hu − *Department of Materials Science and Engineering, University of Maryland, College Park, Maryland 20742, United States; Center for Materials Innovation, University of Maryland, College Park, Maryland 20742, United States;* orcid.org/0000-0002-9456-9315; Email: binghu@umd.edu

Authors

Min Hong − *Department of Materials Science and Engineering, University of Maryland, College Park, Maryland 20742, United States*

Qi Dong − *Department of Materials Science and Engineering, University of Maryland, College Park, Maryland 20742, United States*

Hua Xie − *Department of Materials Science and Engineering, University of Maryland, College Park, Maryland 20742, United States*

Bryson Callie Clifford − *Department of Materials Science and Engineering, University of Maryland, College Park, Maryland 20742, United States*

Ji Qian − *Department of Materials Science and Engineering, University of Maryland, College Park, Maryland 20742, United States*

Xizheng Wang − *Department of Materials Science and Engineering, University of Maryland, College Park, Maryland 20742, United States*

Jian Luo − *Department of NanoEngineering, University of California San Diego, La Jolla, California 92093, United States*

Complete contact information is available at: https://pubs.acs.org/10.1021/acsenergylett.1c01554

Author Contributions

‖M.H., Q.D., and H.X. contributed equally.

Author Contributions

L.H. conceived the idea. M.H. and Q.D. designed the experiments. M.H., H.X., Q.D., and B.C. carried out the experiment with the help of J.Q. and X.W. M.H. and Q.D. collectively wrote the paper with input from all authors. J.L. analyzed the sintering results and mechanism. L.H. supervised the study. All authors discussed the results and contributed to the final manuscript.

Notes

The authors declare no competing financial interest.

■ ACKNOWLEDGMENTS

This work is not funded. The authors gratefully thank the Maryland NanoCenter, the Surface Analysis Center, and the AIM Lab.

■ REFERENCES

(1) Goodenough, J. B.; Park, K. S. The Li-ion rechargeable battery: a perspective. *J. Am. Chem. Soc.* **2013**, *135*, 1167−1176.

(2) Liu, Y. Y.; Zhu, Y. Y.; Cui, Y. Challenges and opportunities towards fast-charging battery materials. *Nat. Energy* **2019**, *4*, 540−550.

(3) Balaish, M.; Gonzalez-Rosillo, J. C.; Kim, K. J.; Zhu, Y. T.; Hood, Z. D.; Rupp, J. L. M. Processing thin but robust electrolytes for solid-state batteries. *Nat. Energy* **2021**, *6*, 227−239.

(4) Zhu, Y. T.; Gonzalez-Rosillo, J. C.; Balaish, M.; Hood, Z. D.; Kim, K. J.; Rupp, J. L. M. Lithium-film ceramics for solid-state lithionic devices. *Nat. Rev. Mater.* **2021**, *6*, 313−331.

(5) Kim, K. J.; Hinricher, J. J.; Rupp, J. L. M. High energy and long cycles. *Nat. Energy* **2020**, *5*, 278−279.

(6) Fergus, J. W. Ceramic and polymeric solid electrolytes for lithium-ion batteries. *J. Power Sources* **2010**, *195*, 4554−4569.

(7) Jiang, Z. Y.; Wang, S. Q.; Chen, X. Z.; Yang, W. L.; Yao, X.; Hu, X. C.; Han, Q. Y.; Wang, H. H. Tape-Casting $Li_{0.34}La_{0.56}TiO_3$ Ceramic Electrolyte Films Permit High Energy Density of Lithium-Metal Batteries. *Adv. Mater.* **2020**, *32*, 1906221.

(8) Wang, C.; Ping, W.; Bai, Q.; Cui, H.; Hensleigh, R.; Wang, R.; Brozena, A. H.; Xu, Z.; Dai, J.; Pei, Y.; Zheng, C.; Pastel, G.; Gao, J.; Wang, X.; Wang, H.; Zhao, J. C.; Yang, B.; Zheng, X. R.; Luo, J.; Mo, Y.; Dunn, B.; Hu, L. A general method to synthesize and sinter bulk ceramics in seconds. *Science* **2020**, *368*, 521.

(9) Kotobuki, M.; Koishi, M. Preparation of$Li_{1.5}Al_{0.5}Ti_{1.5}(PO_4)_3$. solid electrolyte via a sol−gel route using various Al sources. *Ceram. Int.* **2013**, *39*, 4645−4649.

(10) Zheng, F.; Kotobuki, M.; Song, S. F.; Lai, M. O.; Lu, L. Review on solid electrolytes for all-solid-state lithium-ion batteries. *J. Power Sources* **2018**, *389*, 198−213.

(11) Wu, B. B.; Wang, S. Y.; Lochala, J. H.; Desrochers, D.; Liu, B.; Zhang, W. Q.; Yang, J. H.; Xiao, J. The role of the solid electrolyte interphase layer in preventing Li dendrite growth in solid-state batteries. *Energy Environ. Sci.* **2018**, *11*, 1803.

(12) Shen, F. Y.; Dixit, M. B.; Xiao, X. H.; Hatzell, K. B. Effect of Pore Connectivity on Li Dendrite Propagation within LLZO Electrolytes Observed with Synchrotron X-ray Tomography. *ACS Energy Lett.* **2018**, *3*, 1056−1061.

(13) Liu, X.; Garcia-Mendez, R.; Lupini, A. R.; Cheng, Y.; Hood, Z. D.; Han, F.; Sharafi, A.; Idrobo, J. C.; Dudney, N. J.; Wang, C.; Ma, C.; Sakamoto, J.; Chi, M. Local electronic structure variation resulting in Li 'filament 'formation within solid electrolytes. *Nat. Mater.* **2021**.

(14) Liu, H.; Cheng, X. B.; Huang, J. Q.; Yuan, H.; Lu, Y.; Yan, C.; Zhu, G. L.; Xu, R.; Zhao, C. Z.; Hou, L. P.; He, C. X.; Kaskel, S.;

Zhang, Q. Controlling Dendrite Growth in Solid-State Electrolytes. *ACS Energy Lett.* **2020**, *5*, 833−843.
(15) Sun, M. H.; Liu, T. F.; Yuan, Y. F.; Ling, M.; Xu, N.; Liu, Y. Y.; Yan, L. J.; Li, H.; Liu, C. Y.; Lu, Y. Y.; Shi, Y.; He, Y.; Guo, Y. S.; Tao, X. Y.; Liang, C. D.; Lu, J. Visualizing Lithium Dendrite Formation within Solid-State Electrolytes. *ACS Energy Lett.* **2021**, *6*, 451−458.
(16) Song, Y. L.; Yang, L. Y.; Zhao, W. G.; Wang, Z. J.; Zhao, Y.; Wang, Z. Q.; Zhao, Q. H.; Liu, H.; Pan, F. Revealing the Short-Circuiting Mechanism of Garnet-Based Solid-State Electrolyte. *Adv. Energy Mater.* **2019**, *9*, 1900671.
(17) Zhang, Z. Y.; Gonzalez, A. R.; Choy, K. L. Boron Nitride Enhanced Garnet-Type ($Li_{6.25}Al_{0.25}La_3Zr_2O_{12}$) Ceramic Electrolyte for an All-Solid-State Lithium-Ion Battery. *ACS Appl. Energy Mater.* **2019**, *2*, 7438−7448.
(18) Ohta, S.; Seki, J.; Yagi, Y.; Kihira, Y.; Tani, T.; Asaoka, T. Co-sinterable lithium garnet-type oxide electrolyte with cathode for all-solid-state lithium ion battery. *J. Power Sources* **2014**, *265*, 40−44.
(19) Rosero-Navarro, N.; Yamashita, T.; Miura, A.; Higuchi, M.; Tadanaga, K. Effect of sintering additives on relative density and Li-ion conductivity of Nb-doped $Li_7La_3Zr_2O_{12}$ solid electrolyte. *J. Am. Ceram. Soc.* **2017**, *100*, 276−285.
(20) Lin, J.; Wu, L. B.; Huang, Z.; Xu, X. X.; Liu, J. H. $La_2Zr_2O_7$ and MgO co-doped composite Li-Garnet solid electrolyte. *J. Energy Chem.* **2020**, *40*, 132−136.
(21) Li, Y. T.; Xu, B. Y.; Xu, H. H.; Duan, H. N.; Lu, X. J.; Xin, S.; Zhou, W. D.; Xue, L. G.; Fu, G. T.; Manthiram, A.; Goodenough, J. B. Hybrid Polymer/Garnet Electrolyte with a Small Interfacial Resistance for Lithium-Ion Batteries. *Angew. Chem., Int. Ed.* **2017**, *56*, 753−756.
(22) Zhang, Z. S.; Zhang, L.; Yu, C.; Yan, X. L.; Xu, B.; Wang, L. M. Lithium halide coating as an effective intergrain engineering for garnet-type solid electrolytes avoiding high temperature sintering. *Electrochim. Acta* **2018**, *289*, 254−263.
(23) Xu, B. Y.; Li, W. L.; Duan, H. N.; Wang, H. J.; Guo, Y. P.; Li, H.; Liu, H. Z. Li_3PO_4-added garnet-type $Li_{6.5}La_3Zr_{1.5}Ta_{0.5}O_{12}$ for Li-dendrite suppression. *J. Power Sources* **2017**, *354*, 68−73.
(24) Yang, L.; Huang, X.; Zou, C. F.; Tao, X. Y.; Liu, L.; Luo, K. L.; Zeng, P.; Dai, Q. S.; Li, Y. F.; Yi, L. G.; Luo, Z. G.; Wang, X. Y. Rapid preparation and performances of garnet electrolyte with sintering aids for solid-state Li−S battery. *Ceram. Int.* **2021**, *47*, 18196−18204.
(25) Wang, Z. Y.; Kou, Z. Y.; Miao, C.; Xiao, W. Improved performance all-solid-state electrolytes with high compacted density of monodispersed spherical $Li_{1.3}Al_{0.3}Ti_{1.7}(PO_4)_3$ particles. *Ceram. Int.* **2019**, *45*, 14469−14473.
(26) Ping, W. W.; Wang, C. W.; Wang, R. L.; Dong, Q.; Lin, Z. W.; Brozena, A. H.; Dai, J. Q.; Luo, J.; Hu, L. B. Printable, high-performance solid-state electrolyte films. *Sci. Adv.* **2020**, *6*, 8641.
(27) Li, Y. B.; Sun, Y. M.; Pei, A.; Chen, K. F.; Vailionis, A.; Li, Y. Z.; Zheng, G. Y.; Sun, J.; Cui, Y. Robust Pinhole-free Li_3N Solid Electrolyte Grown from Molten Lithium. *ACS Cent. Sci.* **2018**, *4*, 97−104.
(28) Pfenninger, R.; Struzik, M.; Garbayo, I.; Stilp, E.; Rupp, J. L. M. A low ride on processing temperature for fast lithium conduction in garnet solid-state battery films. *Nat. Energy* **2019**, *4*, 475−483.
(29) Li, W.; Wu, G. T.; Araujo, C. M.; Scheicher, R. H.; Blomqvist, A.; Ahuja, R.; Xiong, Z. T.; Feng, Y. P.; Chen, P. Li^+ ion conductivity and diffusion mechanism in α-Li_3N and β-Li_3N. *Energy Environ. Sci.* **2010**, *3*, 1524−1530.
(30) Hong, M.; Dong, Q.; Xie, H.; Wang, X. Z.; Brozena, A. H.; Gao, J. L.; Wang, C. W.; Chen, C. J.; Rao, J. C.; Luo, J.; Hu, L. B. Tailoring grain growth and densification toward a high-performance solid-state electrolyte membrane. *Mater. Today* **2021**, *42*, 41−48.
(31) German, R. M.; Suri, P.; Park, S. J. Review: liquid phase sintering. *J. Mater. Sci.* **2009**, *44*, 1−39.
(32) Noi, K.; Suzuki, K.; Tanibata, N.; Hayashi, A.; Tatsumisago, M. Liquid-phase sintering of highly Na^+ ion conducting $Na_3Zr_2Si_2PO_{12}$ ceramics using Na_3BO_3 additive. *J. Am. Ceram. Soc.* **2018**, *101*, 1255−1265.
(33) Li, Y. Q.; Cao, Y.; Guo, X. X. Influence of lithium oxide additives on densification and ionic conductivity of garnet-type $Li_{6.75}La_3Zr_{1.75}Ta_{0.25}O_{12}$ solid electrolytes. *Solid State Ionics* **2013**, *253*, 76−80.
(34) Park, K.; Goodenough, J. B. Dendrite-Suppressed Lithium Plating from a Liquid Electrolyte via Wetting of Li_3N. *Adv. Energy Mater.* **2017**, *7*, 1700732.
(35) Sun, J. Q.; He, C. H.; Yao, X. M.; Song, A. Q.; Li, Y. G.; Zhang, Q. H.; Hou, C. Y.; Shi, Q. W.; Wang, H. Z. Hierarchical Composite-Solid-Electrolyte with High Electrochemical Stability and Interfacial Regulation for Boosting Ultra-Stable Lithium Batteries. *Adv. Funct. Mater.* **2021**, *31*, 2006381.
(36) Huang, Y.; Chen, B.; Duan, J.; Yang, F.; Wang, T. R.; Wang, Z. F.; Yang, W. J.; Hu, C. C.; Luo, W.; Huang, Y. H. Graphitic Carbon Nitride (g-C_3N_4): An Interface Enabler for Solid-State Lithium Metal Batteries. *Angew. Chem., Int. Ed.* **2020**, *59*, 3699−3704.
(37) Shi, K.; Wan, Z. P.; Yang, L.; Zhang, Y. W.; Huang, Y. F.; Su, S. M.; Xia, H. Y.; Jiang, K. L.; Shen, L.; Hu, Y.; Zhang, S. Q.; Yu, J.; Ren, F. Z.; He, Y. B.; Kang, F. Y. In Situ Construction of an Ultra-Stable Conductive Composite Interface for High-Voltage All-Solid-State Lithium Metal Batteries. *Angew. Chem., Int. Ed.* **2020**, *59*, 11784−11788.
(38) Li, Y. T.; Chen, X.; Dolocan, A.; Cui, Z. M.; Xin, S.; Xue, L. G.; Xu, H. H.; Park, K.; Goodenough, J. B. Garnet Electrolyte with an Ultralow Interfacial Resistance for Li-Metal Batteries. *J. Am. Chem. Soc.* **2018**, *140*, 6448−6455.
(39) Han, F. D.; Westover, A. S.; Yue, J.; Fan, X. L.; Wang, F.; Chi, M. F.; Leonard, D. N.; Dudney, N. J.; Wang, H.; Wang, C. S. High electronic conductivity as the origin of lithium dendrite formation within solid electrolytes. *Nat. Energy* **2019**, *4*, 187−196.
(40) Song, Y. L.; Yang, L. Y.; Tao, L.; Zhao, Q. H.; Wang, Z. J.; Cui, Y. H.; Liu, H.; Lin, Y.; Pan, F. Probing into the origin of an electronic conductivity surge in a garnet solid-state electrolyte. *J. Mater. Chem. A* **2019**, *7*, 22898.
(41) Zhang, P.; Wang, H.; Si, Q.; Matsui, M.; Takeda, Y.; Yamamoto, O.; Imanishi, N. High lithium ion conductivity solid electrolyte of chromium and aluminum co-doped NASICON-type $LiTi_2(PO_4)_3$. *Solid State Ionics* **2015**, *272*, 101−106.
(42) Xie, H.; Bao, Y. H.; Cheng, J.; Wang, C. W.; Hitz, E. M.; Yang, C. P.; Liang, Z. Q.; Zhou, Y. B.; He, S. M.; Li, T.; Hu, L. B. Flexible Garnet Solid-State Electrolyte Membranes Enabled by Tile-and-Grout Design. *ACS Energy Lett.* **2019**, *4*, 2668−2674.
(43) Xie, H.; Hong, M.; Hitz, E. M.; Wang, X. Z.; Cui, M. J.; Kline, D. J.; Zachariah, M. R.; Hu, L. B. High-Temperature Pulse Method for Nanoparticle Redispersion. *J. Am. Chem. Soc.* **2020**, *142*, 17364−17371.

https://doi.org/10.1021/acsenergylett.1c01554
ACS Energy Lett. 2021, 6, 3753−3760